Solar Phys (2007) 245: 287–309
DOI 10.1007/s11207-007-9045-z

Filament Kinking and Its Implications for Eruption and Re-formation

Holly R. Gilbert · David Alexander · Rui Liu

Received: 30 March 2007 / Accepted: 7 September 2007 / Published online: 10 November 2007

Abstract Solar filaments exhibit a range of eruptive-like dynamic activity from the full, or partial, eruption of the filament mass and surrounding magnetic structure, as a CME, to a fully confined dynamic evolution or "failed" eruption, sometimes producing a flare but no CME. Additionally, observations of erupting filaments often show a clear helical structure, indicating the presence of a magnetic flux rope. Dynamic helical structures, in addition to being twisted, frequently show evidence of being kinked, with the axis of the flux rope exhibiting a large-scale writhe. Motivated by the fact that kinking motions are also detected in filaments that fail to erupt, we investigate the possible relationship between the kinking of a filament and its success or failure to erupt. We present an analysis of kinking in filaments and its implications for other filament phenomena such as the nature of the eruption, eruptive acceleration, and post-eruptive re-formation. We elucidate the relationship between kinking and the various filament phenomena via a simple physical picture of the forces involved in kinking together with specific definitions of the types of filament eruption. The present study offers results directly applicable to observations, allowing a thorough exploration of the implications of the observational relationship between kinking and filament phenomena and provides new insight for modelers of CME initiation.

Keywords Filament · Kinking · Eruption · Reformation

1. Introduction

Although coronal mass ejections (CMEs) have been studied for decades, controversies continue as to the exact nature of the driver and initiation mechanism of these energetic eruptions. CMEs frequently exhibit a three-part structure and typically have masses of the order of $10^{15} - 10^{16}$ g, inferred from white-light coronagraph observations. The typical three-part structure observed in white light comprises a bright leading shell of material surrounding a dark cavity within which bright prominence material is found (Crifo, Picat, and Cailloux, 1983; Hundhausen, 1988). Coronal mass ejections are intimately related to erupting

H.R. Gilbert (✉) · D. Alexander · R. Liu
Department of Physics and Astronomy, Rice University, Houston, TX 77005, USA
e-mail: hgilbert@rice.edu

prominences (Sheeley *et al.*, 1975; Munro *et al.*, 1979; Howard *et al.*, 1985; Webb and Hundhausen, 1987; St. Cyr and Webb, 1991; St. Cyr *et al.*, 1999; Gilbert *et al.*, 2000) but the exact nature of this relationship and its importance to the initiation process is still being explored. There is substantial observational evidence supporting the existence of helical flux ropes in solar eruptions such as CMEs and erupting prominences. Figure 1a shows one of the most famous examples, called the "Granddaddy" eruptive prominence, of 4 June 1946 observed at the High Altitude Observatory Climax Station along with a more recent example from 23 April 2001 (Figure 1b) observed at the Mauna Loa Solar Observatory (MLSO). The concept of magnetic flux ropes, helical structures of magnetic field lines, has been used by modelers to describe a variety of solar phenomena (see Lin, Soon, and Baliunas, 2003). Flux rope models of magnetic topology congruously explain prominence support and the existence of a lower density coronal region surrounding a prominence called the cavity. Cavities are often seen in coronal observations of helmet streamers (Tandberg-Hanssen, 1974), but they are

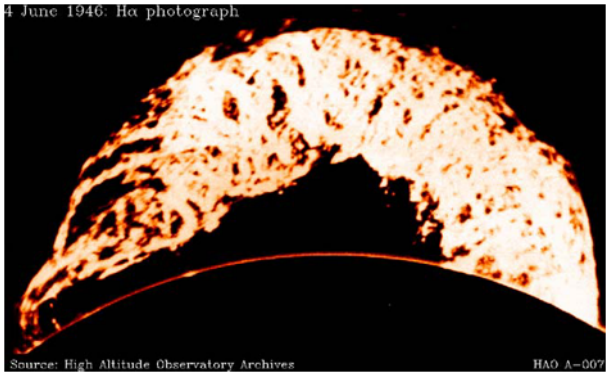

(a)

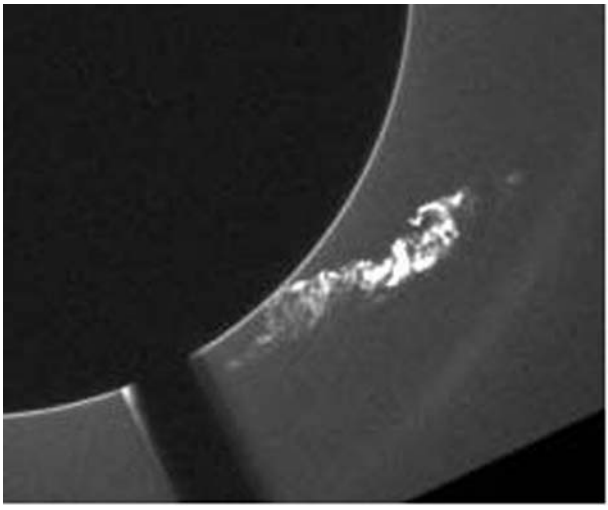

(b)

Figure 1 Large erupting prominences showing helical structure observed in Hα. (a) The "Granddaddy" erupting prominence on 4 June 1946 observed at the High Altitude Observatory Climax Station. (b) A more recent prominence on 23 April 2001 observed at the Mauna Loa Solar Observatory.

most dramatically observed in low-corona white-light observations such as those provided by the Mk4 instrument at MLSO (Gibson *et al.*, 2006). A coronal flux rope configuration with many twists effectively thermally isolates the nonanchored part of the rope (the central section) from the hot corona, thus allowing a cooler condensation to form and settle at the bottom of the flux rope while emptying the surrounding region of hot material, producing the cavity (Low, 1996). Although observations strongly support the existence of magnetic flux ropes in erupting phenomena, controversy remains regarding whether flux ropes exist in the Sun's atmosphere prior to eruption or result as a consequence of magnetic reconnection driven by the eruption. Although there are prominence models that do not require a flux rope configuration but rely instead on dipped field geometries (Kippenhahn and Schlüter, 1957; Antiochos and Klimchuk, 1991), we focus here on flux ropes as these provide a natural topology in which to consider kinking motions.

A necessary component of helical field is the presence of twist, which in a flux rope configuration is generally defined as a measure of the number of windings the field lines make about the flux rope axis. Some simulations of CMEs make use of the large amounts of free magnetic energy stored in pre-eruption twisted magnetic fields prior to release to account for the initiation process (Linker *et al.*, 2003; Fan, 2005). A motion exhibited by flux ropes, intimately related to twist via helicity conservation, is writhing, or the tendency of the axis of the rope itself to twist and form a kink. Some erupting prominences observed in white light and Hα show obvious kinking motions (Figure 2). Many studies have focused on the phenomenon of kinking both numerically (Baty, 2001; Gerrard *et al.*, 2001; Fan and Gibson, 2004; Fan, 2005; Török and Kliem, 2005) and observationally (Sakurai, 1976; Romano, Contarino, and Zuccarello, 2003; Williams *et al.*, 2005; Rust and LaBonte, 2005; Liu, Alexander, and Gilbert, 2007).

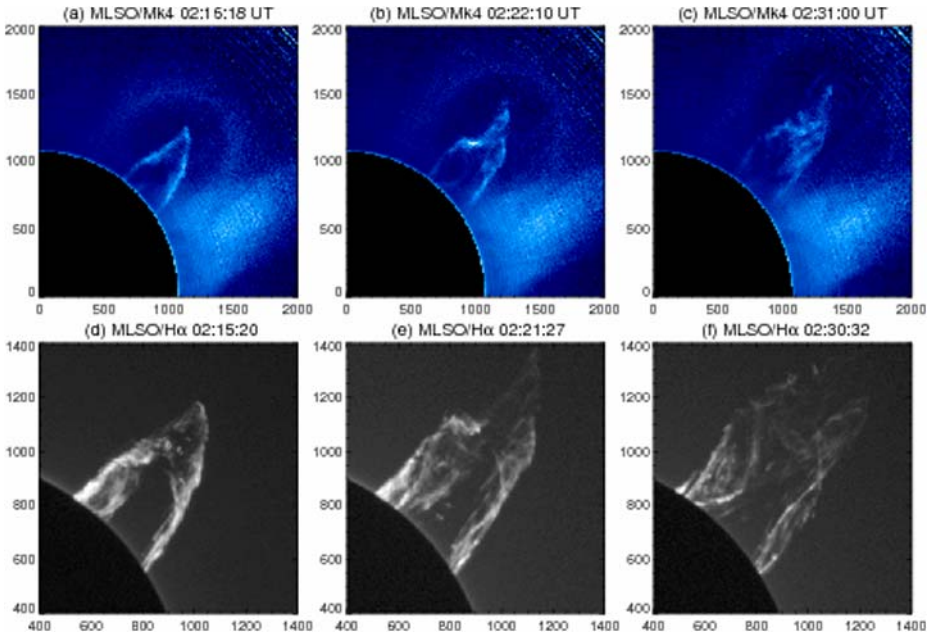

Figure 2 Large erupting prominence and CME showing helical structure and kinking on 18 February 2003 observed in white light data provided by the Mk4 instrument at MLSO (top row) and Hα limb data provided by the PICS instrument at MLSO (bottom row).

Magnetic helicity in flux ropes provides a measure of helical structure and can be estimated via the combination of twist and writhe of the flux tube, that is, $H_m = (T + W)\phi^2$, where T is the number of turns of the field about the axis, W is the number of times the axis loops on itself, and ϕ is the axial magnetic flux in the flux rope. It was proposed by Taylor (1974, 1986) that magnetic helicity is conserved in closed magnetic volumes in ideal MHD. Past theoretical work on kinking in magnetic solar flux ropes involves the initiation of solar eruptions owing to the MHD helical kink instability, which may occur in twisted flux ropes threading the corona that have exceeded some critical threshold of twist (Hood and Priest, 1979). Ideal MHD instabilities such as the kink instability, the torus instability (Kliem and Török, 2006), and the ballooning instability (*e.g.*, Fong, Hurricane, and Cowley, 2001) are just one type of possible mechanism responsible for CME initiation. Other eruption mechanisms include "tether cutting," an intricate part of the catastrophe model (Isenberg, Forbes, and Démoulin, 1993; Lin *et al.*, 1998), and "tether straining," a key factor in the magnetic breakout model of Antiochos, DeVore, and Klimchuk (1999), both of which focus on reconnection as the driver of eruption. These initiation processes are not mutually exclusive since, for example, the kink instability may be occurring in conjunction with a breakout scenario (Williams *et al.*, 2005).

Although the kink instability can be an important component of CMEs, observations also show that significant kinking occurs in filaments that fail to erupt. More recently, kinking has been observed in nonerupting filaments using high-resolution TRACE data (Ji *et al.*, 2003; Alexander, Liu, and Gilbert, 2006). Such nonerupting filaments fit into one end of a categorical range of eruptive-like behavior seen in filament observations. The other categories include cases where all (*full eruption*) or part (*partial eruption*) of the mass may be ejected from the low corona (Gilbert *et al.*, 2000). The range of eruptive-like behavior in filaments and the importance of their dynamic nature to the success or failure to erupt and initiate a CME are still being explored. For example, one must also consider the full magnetic structure, of which the filament is only a part, as it is the interaction of this structure with the ambient corona that drives CME initiation (*e.g.*, Liu, Alexander, and Gilbert, 2007). Observations show that filament kinking is associated with all types of eruption, but it is not clear what role the kinking plays in initiating an eruption or how the degree of kinking relates to the nature of the eruption. A number of recent studies are starting to address this issue (Romano, Contarino, and Zuccarello, 2003; Williams *et al.*, 2005; Alexander, Liu, and Gilbert, 2006; Zhou *et al.*, 2006; Liu, Alexander, and Gilbert, 2007).

Observations of kinking indicate that it is an important physical process at work in filament eruptions, and an understanding of this phenomenon might help to explain how filaments interact with their magnetic environment and what conditions lead to their confinement or result in their eruption. We begin our investigation into this question by offering an observational analysis of the kinking process and its relationship to the different categories of filament eruption in the present paper. We start with a simple physical description of the forces involved in the kinking phenomenon (Section 2), with a more detailed description given in the Appendix. This will be used to develop an understanding of how this process applies to filament eruptions. Second, to better understand the differences between kinking and nonkinking filaments and how they are related to different types of eruption, we establish clear observational definitions of filament kinking and the categories describing the range of eruption (Section 3). This allows us to explore the implications of the kinking process for filament dynamics, including the frequently neglected phenomenon of re-formation[1] (Section 4). Lastly, we present our conclusions in Section 5. A key component in developing an

[1] An observational consequence of partial or failed filament eruptions not generally addressed by models is the apparent "re-formation" of filament material within the same region from which it erupted. The observational

understanding of eruptive behavior is to establish the role played by the prominence magnetic topology in determining the nature of the prominence eruption. Therefore, it is useful to develop clear definitions that can be applied in a general way to observations of kinking and erupting filaments.

2. A Simple Picture of Kinking

Many studies offer a detailed description of the kinking phenomenon in the context of numerical models (Linton, Longcope, and Fisher, 1996; Török, Kliem, and Titov, 2004; Fan, 2005), but our goal here is to explore the role of kinking by developing a picture that can be applied to observations. The kink instability has historically been studied in both solar and plasma fusion contexts. As early as 1968 Anzer considered the stability of solar magnetic cylindrical fields by performing a stability analysis for a periodic perturbation on an infinite flux rope, finding it susceptible to the kink instability. Raadu (1972) found that the cylindrical fields of Anzer (1968) could always be stabilized to the kink instability by taking a sufficiently short length of flux rope and applying rigid boundary conditions at the ends. Parker (1975) discussed twisted flux tubes leading to kinks and the implications for X-ray bright spots on the Sun, and other studies have considered the role of the kink instability in flares (Hood and Priest, 1979; Priest, 1983). The role of the kink instability in interpreting prominence motions and eruption was explored by Sakurai (1976), who found the most important factor in the loss of stability to be the "winding up" of the footpoints. The kink instability is also a phenomenon of interest in plasma fusion research (see, *e.g.*, Biskamp, 1993), where the stability of current-carrying force-free (or nearly force-free) fields has been extensively studied for toroidal geometries, typically with periodic boundary conditions (*e.g.,* Goedbloed and Poedts, 2004). The kinking process and its relation to instabilities is clearly described in theoretical models, but it is more difficult to understand this relationship in the context of solar observations. The question of whether the catastrophic change leading to an eruption requires an instability (Hood and Priest, 1979; Priest and Forbes, 2000) remains one of the key issues associated with kinking flux tubes and is discussed in further detail in Section 4.1.

To address the difficulty of using observations to relate the kinking process to instabilities and to define their role in eruption, we review some of the basic physics behind the forces involved in kinking and the conditions that lead to an instability, the details of which are presented in the Appendix. To summarize briefly, consider an initially straight (*i.e.*, cylindrically symmetric) flux tube that experiences some force (*e.g.*, buoyancy) resulting in the upward displacement that produces a curvature of the axis, or bending of the tube while the footpoints remain fixed. This type of curvature on a straight flux tube axis produces effects that lead to torques where there previously were none, resulting in a writhing of the flux rope. If the resultant force on the flux tube is in the direction of the initial displacement, then the system becomes kink unstable (Boyd and Sanderson, 2003, Section 4.5). If, however, the resultant force on the flux rope axis is in the direction opposite that of the initial displacement, then the system is stable against the kink mode. The force that tends to drive the instability arises from the azimuthal (θ) component of the magnetic field, because this component is enhanced toward the base of the curved flux rope and reduced toward the top. The stabilizing forces are those arising from the axial (z) component of the magnetic field,

relationship between kinking in full, partial, and failed filament eruptions and the re-formation of new material following eruption has not yet been investigated.

which exert a downward tension force in response to the initial displacement. So, in general, if B_θ is sufficiently large in comparison with B_z, the flux rope is kink unstable. The basic picture presented in the Appendix demonstrates that there are forces that can produce a writhing of a magnetic flux rope and that there are a number of other forces that will tend to resist this writhing once it has begun. The relative importance of these various forces will depend on the detailed nature of the initial equilibrium of the flux rope. This can really only be understood thoroughly by performing a systematic numerical study of a broad range of initial equilibria and their nonlinear evolution. In the absence of such a study, we must conclude that a broad range of kinking behavior is possible, and a focused observational study of prominence eruptions (including failed eruptions) can provide important constraints on the range of such behavior that is realized in the solar context.

3. Observational Definitions

A primary objective of the present work is to understand observationally the varying degrees of kinking exhibited by filaments to characterize the different configurations and to determine the relationship between the degree of kinking and the ability of the filament to erupt. It is presently unclear whether the degree of kinking is related to the eruption or not: theoretically the degree of kinking may influence the ability of the filament to erupt (Fan, 2005) or the degree of kinking in an eruption might be determined by the magnetic configuration (T. Török, private communication); observationally this study has not yet been performed.

To understand this possible relationship we need to establish clear observational definitions of kinking and the various types of eruption observed (full, partial, or failed). It is worth noting that when discussing kinking filaments observationally, we assume that the filament is undergoing some form of dynamic evolution. Although it is possible to have a stable kinked configuration, as a result of the evolution of a magnetic system (flux rope and overlying field; see Fan, 2005), we question whether this type of configuration would be detectable in observations because filament material residing in a kinked, stable filament channel may completely drain after a short amount of time. In this work, we concentrate on the observational consequences of kinking filaments where the dynamic evolution is critical.

3.1. Kinking

As mentioned previously, a magnetic flux rope experiences kinking when writhing occurs, or the axis of the rope loops around on itself; that is, writhing can be thought of as the helicity of the axis itself (Berger, 1999). The conversion of twist to writhe can result in a stable kinked configuration, which remains in equilibrium (Fan, 2005) or, for an amount of twist above some critical threshold, result in the development of the kink instability. Converting the theoretical definition of kinking flux tubes into a useful observational tool to study kinking filaments is challenging. In particular, projection effects make it difficult to determine the degree of kinking present, except in the most favorable orientations (*e.g.*, when a kinking filament is observed at disk center the observer's line of sight provides a complete view of the filament axis). Another limitation of observations in determining the degree of kinking arises if only part of the kinking evolution is observed, as in the case where only observations at relatively low heights (*e.g.*, with TRACE) are available. The simulations of Török and Kliem (2005) indicate that two flux ropes with the same amount of initial twist but embedded in different strength ambient coronal field can result in the confinement of one (where the ambient field is stronger) and the eruption of the other. These

simulations exemplify the importance of observing the entire height range within which the conversion of twist into writhe takes place to accurately determine the degree of kinking and its importance. For these two cases, the confined flux rope would show much stronger kinking at low heights than the other since only a small fraction of the overall evolution of the erupting flux rope is visible.

The three-dimensional nature of kinking flux ropes has been studied in the context of numerical MHD simulations (*e.g.*, Fan and Gibson, 2004) with a focus on the appearance of the flux rope from different observational perspectives (Gibson and Low, 2000; Gibson *et al.*, 2004; Fan, 2005). As discussed in those theoretical papers, the orientation of the magnetic flux rope axis with respect to the observer has a significant impact on the projected appearance of the flux rope geometry. When highly kinking filaments are observed at locations away from disk center, the geometry that provides the optimum orientation for observing the kink is where there is a 90-degree angle between the orientation of the rope axis prior to kinking motion and the observer. A flux rope showing significant kinking motion (apex rotations of significantly more than 90 degrees) when observed in projection will exhibit a clear "inverted gamma" shape formed by the apparent crossing of the two filament legs. From this perspective, the projected closed-loop structure above the apparent leg crossing is easily distinguishable (Figure 3). However, the same kinking flux rope observed from a viewpoint parallel to the axis of the spine prior to kinking (0-degree separation between the axis and observer), will, in general, not show such an obviously closed-loop structure, deceptively appearing as a nonkinking filament. The upper portion of the filament in this latter orientation will seem to widen along the filament axis as the kinking occurs, but unless it significantly expands allowing a closed-loop structure to become visible, it would be

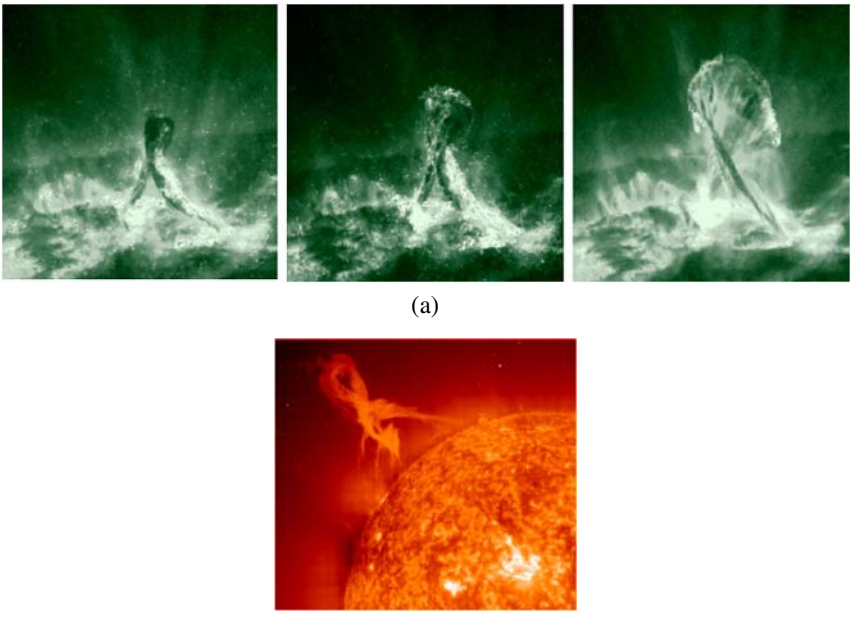

Figure 3 (a) Failed filament eruption on 27 May 2002 showing an "inverted gamma" structure as a result of significant kinking observed in TRACE 19.5 nm. (b) Filament eruption observed by SOHO EIT 30.4 nm on 18 January 2000 also showing an obvious inverted gamma structure.

extremely difficult to use this as a definitive signature of kinking. Gibson and Low (2000) illustrate the difference in appearance between a magnetic flux rope observed on the solar disk as a sigmoidal structure and one observed at the limb perpendicular to the flux rope axis as it takes off as a CME (see their Plate 6). The same line-of-sight issues arise for filaments in kinking configurations, and it is clear then that intensity data alone are not sufficient to infer that a filament is kinking unless the orientation is close to the more favorable orientation. Fortunately, the motion associated with the writhe of the axis will have a distinctive velocity signature, which when combined with intensity observations provides a more definitive test. For example, He I (λ 10830) intensity data from MLSO can be used in conjunction with He I line-of-sight velocity data taken with the same telescope to determine if this type of expansion of a flux rope is occurring. Together with Hα observations, the He I intensity data can be used to help establish the orientation of the filament spine, and the He I velocity data provide velocity signatures to distinguish kinking from simple expansion. The time sequence of the intensity data can also be useful in distinguishing among expansion, kinking, and draining motions of prominence material (*e.g.*, Liu, Alexander, and Gilbert, 2007). Any intermediate angle of observation between 0 and 90 degrees would produce a mixture of the two geometries that would require a combination of time series intensity and Doppler velocity data. It is clearly important to establish the initial orientation of the filament prior to any kinking activity to properly interpret the velocity and intensity data.

Although the existence of an apparent closed-loop structure above the projected crossing of the filament legs is strong evidence of kinking, the situation is further complicated by the requirement that to determine the magnetic structure there must be mass present. If the

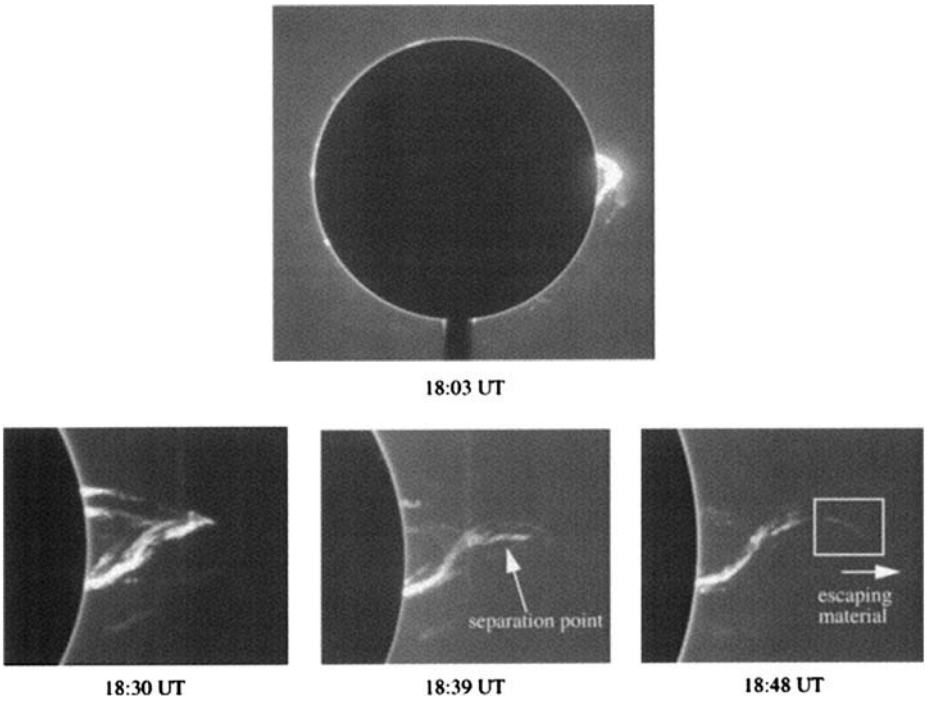

Figure 4 Erupting prominence observed in Hα at MLSO on 21 April 1998 showing a cusp-like structure and a partial eruption (from Gilbert *et al.*, 2000).

kinked portion of the filament spine is not completely filled with material then clear signatures may not be present. Figure 4 shows an example of a kinking structure, as evidenced by its early behavior, which evolves to form the appearance of a linear cusp-like configuration by virtue of the fact that the mass has completely drained from one leg. To be useful, our observational definitions of kinking must account for the degree to which kinking is occurring in addition to allowing for projection effects and nonuniform distributions of material within the kinking flux rope. Observations have shown evidence for a range of kinking, from minor writhing, to a 90-degree turn or more of the axis (with the direction of the writhe applying to the filament apex). Even if the orientation is at its most favorable, a flux tube with only a small amount of writhe may not produce an identifiable signature of the kink. To aid in the identification and quantification of kinking from an observational standpoint, we present the following criteria as a guide for application to observations with the assumption that the orientation of the filament axis, with respect to the observer, is known. For example, the orientation can be determined by Hα observations of the filament prior to the onset of kinking motion. The first challenge is to identify certain observational signatures that indicate whether kinking of the filament axis is occurring. Three cases are to be considered:

Clear Kinked Structure An identifiable closed-loop is evident above two filament legs that are clearly separated from each other and anchored to the surface. If the line of sight of the observer relative to the initial orientation of the filament axis is less than 45 degrees, as measured in the direction of the writhe of the apex (see Figure 5a, where 0 degrees applies to the case where the filament axis is parallel to the line of sight of the observer, and 90 degrees is the perpendicular case) and a clear closed-loop structure exists, then there is a large amount of kinking (*i.e.*, 90-degree kink; see Figure 5b and corresponding discussion in the following).

Possible Kinked Structure In the absence of an identifiable closed-loop structure, a cusp-like structure forms above two filament legs anchored to the surface while writhing motions are apparent in the dynamical process of eruption. If the line of sight of the observer relative to the initial orientation of the filament axis is less than 45 degrees, as measured in the direction of the writhe of the apex, and a clear cusp-like structure exists, this is probably indicative of a large degree of kinking. Velocity information is needed here to establish whether writhing motions are occurring (see Liu, Alexander, and Gilbert, 2007).

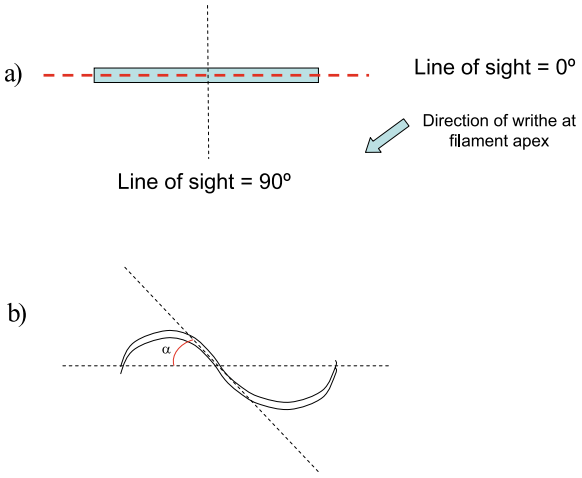

Figure 5 (a) Schematic representing the top view of an unkinked filament. The plane connecting the two footpoints and the center of the Sun (located directly below the filament) is shown by the red dashed line. (b) Top view of a kinked filament with intersecting planes shown as dashed lines. α is the angle between the two planes, measuring the degree of kinking.

Low Evidence of Kinked Structure No closed-loop or cusp structure is visible during the rise of a filament axis, and/or line-of-sight velocity data show a complete absence of writhing motions with or without a projected closed-loop or cusp structure.

In addition, for those events in which there is a clear kinked structure, it is useful to also determine how much they are kinking. To estimate the amount of kinking occurring, we must know the orientation of the pre-eruptive filament and use this information to define a reference plane formed by the two filament footpoints and the center of the Sun. As a filament kinks, we define another plane by two points marking the length of the mid-section of the rising filament and the center of the Sun. It is the angle between these two planes that provide a measure of the kinking (Figure 5). Prior to writhing, the two planes are parallel. If the planes evolve to a point of being perpendicular, we define this as a 90-degree kink. Quantifying the amount of kinking in observations is a challenging task and although a combination of data sets can be utilized in doing so, there will be some degree of uncertainty involved with this type of analysis. The amount of eruptive filament kinking is easiest to establish in those events viewed directly from above (*i.e.*, near center disk) since the angle between the two planes defined above is more accurately determined from this viewpoint (*e.g.*, Figure 5). Observations by STEREO (*Solar Terrestrial Relations Observatory*) combined with the He I (10830 Å) velocity data may help resolve some of the projection effect issues in determining the amount of kinking in filaments and allow a more effective application of the definitions listed here, which were derived from single vantage point observations.

Romano, Contarino, and Zuccarello (2003) defined kinking using the ratio between the pitch of the magnetic field lines and the filament width. For example, they measured a decrease in this ratio in the filament eruption of 19 July 2000, concluding that the filament was kinking. Berger and Field (1984) and Rust and LaBonte (2005) used the pattern of writhe to determine whether kinking is occurring. Previous observational studies of kinking involve the determination of the sense of twist and writhe (and how they are related), or whether the filaments are subject to the kink instability by passing a critical amount of twist (Rust and Kumar, 1994). In contrast, we offer working definitions based on observational examples that demonstrate that there are both similarities and differences between those events that show extreme kinking and those that show minimal kinking.

3.2. Types of Eruption

Our primary goal is to define an observationally based foundation from which to explore the connection, if any, between writhing motions in filaments and their tendency to erupt. Specifically, is there a minimum degree of writhe, or kink, above which eruption is inevitable? Furthermore, does the degree to which the filament kinks determine whether the eruption is full or partial or whether only the filament or cavity erupts?

Prominences have generally been defined in terms of the magnetic environment in which they form (*i.e.*, active region versus quiescent; Martin, 1989; Tandberg-Hanssen, 1974, 1995; Tang, 1987; Zirin, 1988), their shape (*e.g.*, loop prominences), or their dynamics (eruptive versus active; Gilbert *et al.*, 2000). To augment these definitions, we consider further the details of the prominence eruptive behavior. Prominences have been observed to exhibit a wide range of eruptive activity behavior, including dramatic activation with the filament mass remaining confined to the low corona (*e.g.*, Ji *et al.*, 2003; Alexander, Liu, and Gilbert, 2006), the eruption of part of the observed filament structure (*e.g.*, Zhou *et al.*, 2006), and the almost complete eruption of all of the prominence mass (*e.g.*, Plunkett *et al.*, 2000). To gain a better understanding of the varying types of eruption and how they are related, we establish here clear observational definitions that can be applied to prominence eruptions in

Table 1 Summary of filament mass and structure eruption types.

	Type of eruption	Description
1	Full	Bulk ($\geq$ 90%) of filament mass and magnetic structure escapes the Sun
2	Partial	(a) Entire magnetic structure erupts with some or none of the filament mass (as a result of mass draining)
		(b) Partial eruption of the magnetic structure with some or none of the filament mass (as a result of mass draining and/or settling)
3	Failed	None of the filament mass nor magnetic structure escapes the Sun

general, but also in the context of kinking motions. A principal focus of the present work is to discuss, for the class of eruptive filaments involving kinks, how the kinking is related to the eventual nature of the eruption.

Before proceeding, it is instructive to point out that, although the filament mass and the associated supporting magnetic structure are coupled, we distinguish between the two when describing eruptions observationally because the magnetic structure can erupt, destabilizing the corona and generating a CME, while the filament mass remains confined (*e.g.*, Liu, Alexander, and Gilbert, 2007). The flux rope topology adopted here defines a large-scale helical magnetic structure that is able to support filament mass in its lower portions where the field is concave-up. The remaining part of the flux rope is generally devoid of matter and is known as the cavity (Tandberg-Hanssen, 1974; Low, 1996; Gibson *et al.*, 2006). The role played by the dynamical evolution of mass in filaments is, therefore, an important factor in the eventual nature of the eruption and in the subsequent re-formation of the filament (see Section 4.2).

To help elucidate the relation between the filament mass and corresponding supporting magnetic structure, we develop observational definitions of "full," "partial," and "failed" eruptions, of which "partial" is the most complex, summarized in Table 1.

The coupling of the magnetic structure and the filament mass is important in considering eruption, but the mass is most easily observed. We exclude from consideration eruptive behavior in the absence of a pre-eruption filament (*i.e.*, eruption of an empty filament channel) because we are interested here in eruptions driven by kinking motions, and kinking of an empty filament channel with no plasma to outline the field lines would be virtually impossible to observe with current data capabilities. Eruptions of empty cavities are generally difficult to observe, but the definitions provided in the following could be easily extended to include empty filament channels if the appropriate data were available. Since we are interested in dynamic prominences (as opposed to those that slowly rise over several days), we include in our eruptive definitions those events in which a portion of a prominence lifts significantly in a short period of time (at least 0.1 R_s in less than 1 hour). These criteria are based on extensive observational experience with active versus eruptive prominences (Gilbert *et al.*, 2000).

A "full eruption" is defined to occur when the entire magnetic structure erupts while containing the bulk (approximately 90% or more) of the pre-eruptive filament mass (*i.e.*, the mass escapes without draining or settling back to the surface). It is uncertain whether an eruption involving 100% of the filament mass ever occurs since draining is generally observed in erupting events, but to distinguish between "partial" eruptions (described in the following) and the more dramatic large, almost complete eruptions, the choice of 90% of the mass is a reasonable delineation of these two types of events. We specifically address whether it is possible to observe a full eruption subsequent to kinking motion. The optimum

conditions for a rising, kinking flux rope to eject the bulk of the filament material residing within it involve the following: (1) the initial location of all of the filament material must be at the middle section of the rope and (2) the eruption must occur quickly enough so that only a small fraction of the material has time to drain along either leg to the surface. Unfortunately, if these two conditions are fulfilled, it would be difficult to identify the kinking structure as a kinking of the flux rope, because the successful detection of the kinking motion requires the presence of the filament material. We, therefore, conclude that a full eruption, as defined here, is highly unlikely to be detected in observations of kinking structures.

We define the case in which none of the lifted filament mass nor the supporting magnetic structure escapes the solar gravitational field as a "failed eruption," although this does not preclude localized dynamic activity, heating, and flare production (see Figure 1; Alexander, Liu, and Gilbert, 2006). An example of a kinking failed filament eruption demonstrating significant draining occurred on 27 May 2002 and has been studied in detail by Ji *et al.* (2003), Török and Kliem (2005), and Alexander, Liu, and Gilbert (2006). This type of failed eruption has two mechanisms by which mass returns to the surface instead of escaping (also applicable to the partial eruptions discussed in the following): (1) mass draining along apparent magnetic field lines back into the photosphere and (2) mass remaining in concave-upward field lines that "settle" back to a lower altitude in the corona. In the latter scenario, mass does not get lost to the photosphere, but instead it can return with its supporting structure as they both relax in the atmosphere after releasing part of the flux rope (the concave-upward or largely horizontal field lines continue to support the mass), resulting in the filament mass maintaining its presence in the corona. The distinction between these two mechanisms for mass "return" becomes important when considering filament re-formation following eruption (see Section 4.2).

"Partial eruptions" are more complicated to define observationally, since the coupling of the filament mass and its supporting magnetic structure create a couple of different subcategories in this class. The first type of partial eruption occurs when the entire magnetic structure erupts, with the eruption containing either some or none of its supported pre-eruptive filament mass. The mechanism by which mass loss occurs in this scenario is draining along magnetic field lines connected to the photosphere, manifested in observations as an initial lifting of material followed by draining of some or all of the mass, essentially losing it to the photosphere. If the structure were to carry the bulk of the filament mass, only incurring a small fraction of mass loss via draining, this type of eruption would fall under the "full eruption" category. The second type of partial eruption occurs when the magnetic structure itself partially escapes with either some or none of the filament mass. Observationally, this type of partial eruption with no filament mass manifests as a lifting of filament material followed by draining and/or settling back to the surface while reconnection splits the flux rope in two above the apex of the filament, resulting in a failure of the mass to escape but allowing part of the cavity to escape with a resulting CME. (See Section 4.1 for a discussion of the implications of different reconnection locations.) This particular case can be labeled a "partial cavity with failed filament eruption." A similar sequence of events can occur but with reconnection occurring within the filament, creating a partial eruption of material along with the partial eruption of the cavity. This could be called a "partial cavity with partial filament eruption."

4. Implications

Understanding the basic physics involved and establishing clear observational definitions of the kinking process allows us to examine the relationship between kinking and the nature of

eruption. Additionally, establishing clear observational definitions of the types of eruption illuminates an important implication of partial and failed eruptions: the phenomenon of filament re-formation. We closely examine these aspects in the following sections.

4.1. Eruption

As described in the previous section, there are several ways in which a filament and its supporting structure can exhibit eruptive behavior, with or without kinking. While kinking filaments represent a subgroup of erupting prominences, the kinking phenomenon may play an integral role in the success or failure to erupt. Initial results indicate that "failed" events generally demonstrate a large degree of kinking. Moreover, the relationship and fundamental differences between the types of eruption depend crucially on the role played by reconnection in both the eruption and kinking processes. We discuss this relationship by considering the magnetic environment in which the filament occurs and how reconnection participates to produce the range of eruptive activity observed, particularly in the kinking configuration.

The role of topology in determining the varying degrees of eruption can be described concisely by considering a two-dimensional picture of the inverse polarity flux rope prominence model (Kuperus and Raadu, 1974; Pneuman, 1983; Anzer, 1989; Low and Hundhausen, 1995). (The normal polarity flux rope model has the same consequences of reconnection.) As discussed earlier, the flux rope model is naturally applicable to the kinking phenomenon. As illustrated in Figure 6 (from Gilbert *et al.*, 2001) the magnetic topology leading to a full, partial, and failed eruption can be understood by considering where reconnection occurs with respect to the prominence. The location of reconnection and the formation of x-type neutral lines in the two-dimensional flux rope model can occur completely below the prominence and its supporting flux rope, resulting in a full eruption. Reconnection can also occur completely above the prominence (*i.e.*, a failed eruption) or within the flux rope itself,

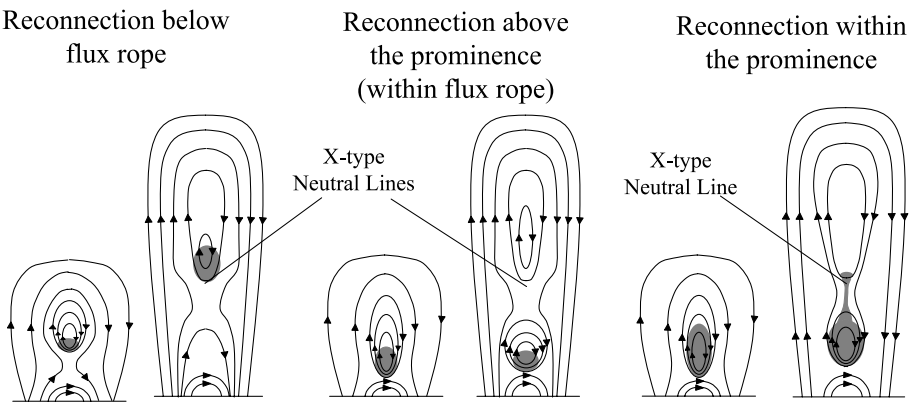

Figure 6 Left: Schematic diagram showing the magnetic topologies of the evolution of an inverse polarity flux rope model during a CME. An x-type neutral line forms below the flux rope following reconnection, leading to a complete eruption of the prominence embedded in the CME. Middle: Schematic diagram showing the magnetic topologies of the evolution of an inverse polarity flux rope model during a CME with horizontal reconnection occurring above the prominence and within the flux rope. An x-type neutral line forms above the original flux rope, creating two flux ropes: the original and one above. No prominence material escapes with the CME in this scenario. Right: Schematic diagram showing the magnetic topologies of the evolution of an inverse polarity flux rope model during a CME with horizontal reconnection occurring within the prominence and within the flux rope. Separation of prominence material occurs through the formation of a second x-type neutral line in the upper portion of the prominence (from Gilbert *et al.*, 2001).

resulting in a partial filament or partial cavity. The physics behind this two-dimensional description readily applies to the three-dimensional models.

Recently, Fan (2005) has developed a numerical MHD model that simulates the coronal magnetic field evolution as a twisted magnetic structure is being transported through the lower boundary into a pre-existing coronal potential field. This "rupture" model of Fan invokes an emerging magnetic flux rope that loses confinement owing to kinking motions as it emerges. Gibson and Fan (2006) extend the simulation long enough in time to show the erupting flux rope breaking into two, and thus only partially erupting. As previously mentioned, one observational consequence of reconnection occurring within the flux rope is that part or none of the filament material escapes (depending on where reconnection occurs relative to the material). The observational definitions of full, partial, and failed eruptions provided in the previous section summarize the various possibilities and can serve as a reference for modelers when comparing their simulations to observations. The Fan (2005) simulation is specific to a kinking flux rope, but the splitting of a flux rope can occur in cases where only lifting is occurring; the difference is the driver of reconnection at the point of separation. For example, in the Gibson and Fan (2006) simulation, reconnection occurs because of the writhing of the flux rope, which brings field lines together in an orientation that is conducive to reconnection. Recently, Alexander, Liu, and Gilbert (2006) demonstrated evidence for this scenario in the failed eruption of 27 May 2002, where writhing motions are associated with reconnection in the region between the two legs of the kinking filament producing a coronal hard X-ray source signifying reconnection-driven energy release. Depending on which flux system is involved in the reconnection, it could have resulted from the crossing of the legs or from the formation of a vertical current sheet below the kinking flux rope. In the case of Török, Kliem, and Titov, 2004, the latter is caused by the pinching of a hyperbolic flux tube (similar to a magnetic X-line in two dimensions) by the flux rope expansion. In a nonkinking eruption, reconnection may be driven by the formation of a current sheet under the rising flux rope (*e.g.*, Lin and Forbes, 2000) or somewhere within the body of the flux rope. We illustrate this latter scenario by considering a positively buoyant coronal flux rope that contains a prominence at its base. The balance of forces between the flux rope and its surroundings may be different between upper and lower portions depending upon importance of mass and strength and variation of the surrounding field. If the region of the prominence is either neutrally or negatively buoyant, the prominence material will tend to lag behind, and possible stay behind the outward moving flux rope. If, however, the CME expansion can produce enough tension force in the field to raise the prominence material sufficiently rapidly, then reconnection can occur initially in the middle of the flux rope structure. In such a scenario, a portion of prominence can get "clipped off" and escape with the CME while the remaining prominence material becomes magnetically disconnected from the CME. This would be a partial eruption. Flux rope splitting can also occur in the absence of prominence material, but it would be extremely difficult to observe with our current observational capabilities.

Török and Kliem (2005) simulated the dynamic behavior of the 27 May 2002 failed eruption event, nicely reproducing both the observed development of the kinking structure and the rise profile of the filament. In this simulation, the upwardly directed kink instability leads to the ascent and helical deformation of a flux rope as well as to the formation of current sheets. They argue that kinking is an important driver in the initial phase of many solar eruptions and the response of a filament to kinking (*i.e.*, failure or success to erupt) is mainly determined by how sharply the overlying magnetic field declines with height. Our observational definitions given in Section 3.1 provide a framework against which these models may be compared and used to guide further developments.

Many of the models that simulate kinking, as well as the observational studies of kinking, depend on the kink instability as a driver of the eruption. Sakurai (1976), however, suggests that the kink instability does not necessarily lead to violent motion but that the "winding up" of the filament footpoints, the most important factor in driving the kink instability, can actually lead to the distortion of an otherwise unstable kink to a more stable helical equilibrium, should such a state exist. Adding more twist, the helical flux rope finds another equilibrium, if any, and so on. A violent instability will arise only if there is no stable neighboring configuration. More recently, three possibilities have been proposed to describe the role that kinking motions play in the eruption process. In the model of Fan (2005) the kinking of the flux rope allows it to "slip through" the overlying arcade fields. In this model, the evolution of the flux rope is governed by the emergence of magnetic flux and proceeds through an early quasistatic stage in which the kinking structure evolves through a series of kinked equilibria. Throughout this stage, neighboring equilibria are reached when the flux emergence is stopped so that the kinking flux rope is governed by the balance of the remaining relevant forces (*i.e.*, the azimuthal, θ, component of the magnetic field, which tends to drive the instability, is balanced by the stabilizing forces arising from the axial, z, component of the magnetic field; see Section 2). Above a critical threshold, the twist of the flux rope results in the onset of the kink instability, facilitating a loss of confinement as the increased kink changes the orientation of the flux rope, allowing it to "slip through" the overlying arcade. A second possibility is that a kinking flux rope may "overshoot" and pass the point at which it is able to slip through the overlying arcade. Consequently, such a flux rope could be confined (*e.g.*, Ji *et al.*, 2003; Alexander, Liu, and Gilbert, 2006). These first two possibilities invoke "slipping" through the arcades as would be necessary for ejection of the flux rope from the Sun as envisaged in the models of Sturrock *et al.* (2001) and Fan (2005). However, flux ropes can also be driven to erupt by other forces. Recently, numerical simulations of the torus instability (Török and Kliem, 2007) have shown that erupting flux ropes need not be aligned with the overlying field to erupt. An observational study of kinking filaments is required to help elucidate the relationship between the differing instabilities and erupting flux ropes. Finally, a kinking flux rope driven by the injection of helicity (*e.g.*, by photosperic motions) may kink to the point where the accumulation of magnetic helicity in the system exceeds an upper bound beyond which no stable equilibrium can be found (see Zhang, Flyer, and Low, 2006). Although the kink instability might play a role in the evolution in this case, it is difficult to determine this observationally since helicity injection can cause a flux rope to twist, expand, and writhe (Amari *et al.*, 1996; Török and Kliem, 2003; Aulanier, Démoulin, and Grappin, 2005) without an instability setting in.

As described in Section 3.2, reconnection plays a critical role in the eruption and the kinking process. Hard X-ray data can be utilized to explore the locations of possible reconnection sites and analyze how this relates to the type of eruption that ensues (*e.g.*, Alexander, Liu, and Gilbert, 2006). Investigating the sources and timing of hard X-ray production leads to a better understanding of the factors involved in filament acceleration and confinement. For example, in determining why a filament may start to rise and accelerate but fail to erupt, we can turn to possible signs of reconnection to establish how the timing and location of reconnection sites relates to either the loss of equilibrium or the stabilization of the filament. Reconnection in the corona above an energized filament may significantly weaken the overlying fields, leading to a possible sudden increase in filament acceleration, facilitating eruption. Acceleration profiles of eruptive filaments coupled with hard X-ray data may provide a more complete picture of how the loss of stability or confinement is related to reconnection in the overall magnetic system.

Understanding the physical conditions leading to full, partial, and failed filament eruptions will enable us to understand the interplay between filaments and the surrounding

magnetic field. A complete picture of kinking filaments involves understanding the driving mechanisms as well as the factors involved in confinement. We are currently conducting an observational study to address the questions raised here. This study applies the observational definitions of Section 3 to a number of erupting prominence events to determine how kinking is related to the dynamics of eruption. To establish this relationship, we consider the degree to which events kink and what role the amount of kinking plays in their success or failure to erupt. Moreover, we also consider whether we can distinguish between events that undergo a kink instability or a kink-induced loss of equilibrium. This observational study will lead to a better general understanding of filaments and how they interact with their surrounding magnetic environment and may also stimulate theoreticians to implement a broad, systematic study that includes a statistically significant number of cases that are relevant to the Sun.

4.2. Re-formation

A phenomenon that is frequently observed (Mouradian and Soru-Escaut, 1989; Schmieder *et al.*, 2006) in filament eruptions, but not discussed in most models, is re-formation of filament material following an eruption. Amari *et al.* (2003) describe the re-formation of a flux rope during a diffusion-driven evolution that remains in equilibrium, thus providing a favorable site for the formation of new filament material. One important implication of partial and failed eruptions is that filament re-formation can be explained, in part, by considering the relationship between magnetic reconnection and the subsequent evolution of the material during eruption. Gibson and Fan (2006) perform a simulation of an erupting flux rope that splits so that some of the dipped field of the original flux rope escapes, and some survives the eruption. The surviving dipped field may also contain filament mass. The phenomenon of filament re-formation is almost exclusively observed in disk observations where filament material will apparently re-form in the same channel on time scales as short as hours following an eruption. In the context of partial and failed eruptions, we can question whether the re-formation process is actually the formation of a new condensation or is just an observational consequence of material settling back down to the surface during a partial or failed eruption. When a partial or failed eruption is observed in Hα disk data, the initial lifting of the filament might occur rapidly enough that its velocity shifts the wavelength of the material out of the narrow passband of Hα filters, thus "disappearing." When the lifting material decelerates and begins to drain and settle (with the amount of draining and/or settling depending on how much of the filament erupts and how much falls under gravity), the settling material will then become visible again, spatially located similarly to the pre-eruption mass. The draining material (*i.e.*, along predominantly vertical field lines) will be lost back to the photosphere, but the settling material will relax along with the supporting structure and remain suspended in the corona. If this type of settling of material is responsible for the apparent re-formation of filaments, then we can conjecture that a failed eruption with relatively little draining would create a more complete refilling of the filament channel than an event where much of the material erupts. A comprehensive observational study is underway to consider the phenomenon of re-formation, utilizing both disk and limb data. It is far less common to observe re-formation of new prominence material at the limb, but it is very common to observe draining and settling of material there. These types of limb observations support the possibility that re-formation is an observational consequence of material settling back toward the surface in partial and failed eruptions, and thus the detailed study of the re-formation process can lead to an important diagnostic for modeling. The nature, time development, and spatial distribution of the filament re-formation provide important constraints on CME initiation models. The simple fact that a filament re-forms tends to support

the class of models where the magnetic configuration and its evolution allows for partial eruptions, as defined here, and the subsequent settling of material to form a new filament.

5. Conclusions

Motivated by observations of filaments that exhibit kinking motions, we have presented a simple view of the kinking process in conjunction with observational examples to establish working definitions of the dynamics of kinking in filaments. We have developed useful definitions of full, partial, and failed filament eruptions, both in kinking and nonkinking contexts, which can be used to augment present definitions of filament activity and to guide modeling efforts. The definitions presented here can be applied generally to filaments and we expect they will prove useful in other observational studies of filament activity. We have identified three main observational considerations that yield insight into the physical processes involved in erupting prominences. These are the presence and degree of writhing motions, the nature of the eruption, and the location and driver of magnetic reconnection. One or other of these processes appear in the various models of flux rope CMEs but not in the detail required for direct comparison with observations. The degree to which a filament is kinking and the location of the reconnection site may determine whether we observe a full, partial, or failed filament eruption. Filaments that either partially erupt or fail to erupt have an observational consequence for what has historically been referred to as "re-formation" following eruption, since some of the material that does not escape settles back in the relaxing structure, giving the illusion that completely new material is forming. These results provide a first step in the investigation into implications of the relationship between kinking and filament phenomena. Although directly applicable to observations, they also provide a framework from which models of flux rope eruptions can incorporate more observationally relevant physics.

Acknowledgements We would like to thank Tibor Török for an extremely thoughtful and useful review of the paper. We also thank B.C. Low, Yuhong Fan, Thomas Holzer, and Tahar Amari for their insightful comments. This work was partially supported by NSF SHINE Grant No. ATM 03-53345.

Appendix

A thorough examination of kinking motion in magnetic flux ropes includes evaluating the divergence of the Maxwell stress tensor to determine the driving $\vec{J} \times \vec{B}$ force. In considering kinking motions in observations, we begin with a simple schematic that represents three simple magnetic geometries (Figure 7) for which we can derive the form of the stress tensor. Geometry (a) has the magnetic field parallel to the z-axis, whereas in the two flux rope cases, (b) and (c), the field has z- and θ-components (b) and ζ- and θ-components (c). Case (a) corresponds to what Boyd and Sanderson (2003, Section 4.3) refer to as the principal axis case, and the total stress tensor for a magnetized fluid in the ideal MHD approximation can be written

$$\overleftrightarrow{\mathcal{T}} = \overleftrightarrow{\mathcal{T}}_{\mathrm{f}} + \overleftrightarrow{\mathcal{T}}_{\mathrm{M}} = \left(p + B^2/2\mu_0\right) \overleftrightarrow{\mathbf{I}} - \vec{\mathbf{B}}\vec{\mathbf{B}}/\mu_0, \tag{1}$$

where $\mathcal{T}_{\mathrm{f}}$ is the fluid stress tensor, $\mathcal{T}_{\mathrm{M}}$ is the Maxwell stress tensor in the nonrelativistic limit, and $\mathbf{I}$ is the unit tensor. It follows from (1) that the components of the total stress tensor, $\overleftrightarrow{\mathcal{T}}$, in case (a) are

$$\mathcal{T}_{ij} = \begin{pmatrix} p + B^2/2\mu_0 & 0 & 0 \\ 0 & p + B^2/2\mu_0 & 0 \\ 0 & 0 & p - B^2/2\mu_0 \end{pmatrix}. \tag{2}$$

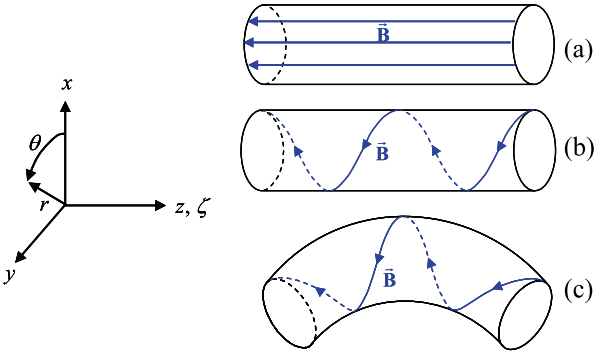

Figure 7 Three magnetic geometries and corresponding useful coordinate systems. In the Cartesian (x, y, z) and cylindrical (r, θ, z) systems ((a) and (b) respectively) the z-axis is the same, while in the third orthogonal coordinate system (r, θ, ζ) the ζ coordinate (which replaces the z coordinate) lies along the axis of the magnetic flux rope, and the $r - \theta$ plane is perpendicular to that axis (c).

In case (b), the magnetic field has both a z-component and a θ-component, so the last term in Equation (1) has the form

$$\vec{\mathbf{B}}\vec{\mathbf{B}}/\mu_0 = \left(B_\theta^2 \hat{\mathbf{e}}_\theta \hat{\mathbf{e}}_\theta + B_z^2 \hat{\mathbf{e}}_z \hat{\mathbf{e}}_z + B_\theta B_z \hat{\mathbf{e}}_\theta \hat{\mathbf{e}}_z + B_\theta B_z \hat{\mathbf{e}}_z \hat{\mathbf{e}}_\theta\right)/\mu_0. \tag{3}$$

Since for this case $B^2 = B_\theta^2 + B_z^2$, it follows from Equations (1) and (3) that the components of the stress tensor are given by

$$\mathcal{T}_{ij} = \begin{pmatrix} p + B^2/2\mu_0 & 0 & 0 \\ 0 & p + (B_z^2 - B_\theta^2)/2\mu_0 & -B_\theta B_z/\mu_0 \\ 0 & -B_\theta B_z/\mu_0 & p + (B_\theta^2 - B_z^2/2\mu_0 \end{pmatrix}. \tag{4}$$

For case (c), a similar analysis yields

$$\mathcal{T}_{ij} = \begin{pmatrix} p + B^2/2\mu_0 & 0 & 0 \\ 0 & p + (B_\zeta^2 - B_\theta^2)/2\mu_0 & -B_\theta B_\zeta/\mu_0 \\ 0 & -B_\theta B_\zeta/\mu_0 & p + (B_\theta^2 - B_\zeta^2)/2\mu_0 \end{pmatrix}. \tag{5}$$

We can now apply these results to the case shown in Figure 7c, and we will thus be concerned only with a surface of constant r and two surfaces of constant ζ.

Consider a small element of a cylindrical magnetic flux rope (Figure 8a) where two coordinate systems are shown: the Cartesian system remains fixed, but the cylindrical system is a local system defined such that the ζ-axis corresponds to the axis of the flux rope and will thus differ from the z-axis as the flux rope is distorted. The exact nature of the lateral stage of the kink instability (in particular, the criterion for stability) depends on the nature of the initial MHD equilibrium (*e.g.*, Boyd and Sanderson, 2003, Section 4.5). We assume our initial equilibrium state has the basic magnetic geometry shown in Figure 8a, namely, a cylindrical magnetic flux rope with a magnetic field characterized by θ- and z-components, an external magnetic field that also has both θ- and z-components, and a finite plasma pressure both inside and outside the flux rope. Since we are dealing with a coronal problem, the low-β assumption (magnetic energy density much larger than plasma energy density) is made, and the effects of plasma pressure are thus ignored. If the cylindrical flux rope of Figure 8a is linearly perturbed into a geometry similar to that shown in Figure 8b, the curvature produces effects that lead to torques where there were none in the rope with a straight axis, and if the resultant force on it is in the direction of the initial displacement, then the system becomes kink unstable (Boyd and Sanderson, 2003, Chapter 4). If, however, the resultant force on the flux rope axis is in the direction opposite that of the initial displacement, then the system is

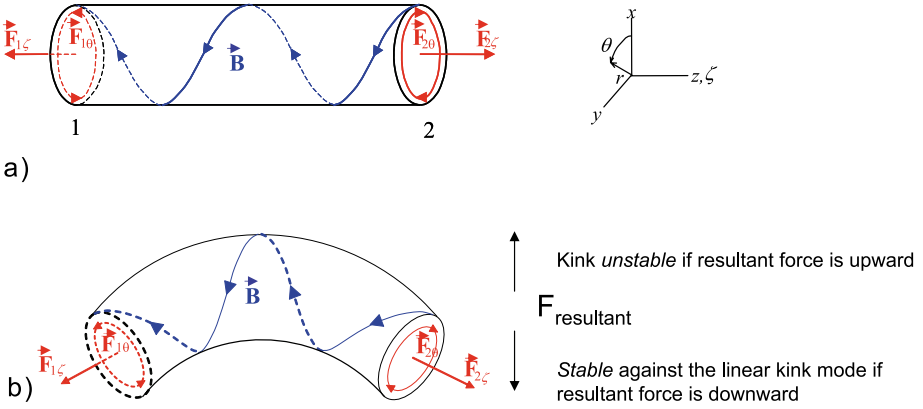

Figure 8 (a) Small element of a cylindrical magnetic flux rope, with the helical magnetic field indicated by a single field line on the outer boundary of the flux rope. Two coordinate systems are shown: a Cartesian system (x, y, z), which remains fixed in space; and a cylindrical system (r, θ, ζ), which is a local system in which the ζ coordinate lies along the local axis of the flux tube. In the case of a cylindrical flux rope, the ζ-axis and the z-axis are the same, but as the flux rope is linearly perturbed and thus distorted (b), the two axes will differ. Shown in red are the magnetic tension forces exerted on the two faces of the cylindrical flux rope element by the magnetic field just outside of each face.

stable against the linear kink mode. The force that tends to drive the instability arises from the θ-component of the magnetic field, because this component is enhanced toward the base of the curved flux rope and reduced toward the top (Figure 8b). The stabilizing forces are those arising from the z-component of the magnetic field, which exert a downward tension force in response to the initial displacement. So, in general, if B_θ is sufficiently large in comparison with B_z, the flux rope is kink unstable. It is worth noting that the lateral stage of the kink instability does not require any writhing of the perturbed flux rope; the writhing occurs as a result of the unbalanced forces caused by the curving of the flux tube (Hood, 1992). If writhing is to occur, it comes in the helical stage of evolution as shown in Figure 9a and discussed in the following. This discussion of the lateral stage of the kink instability deals only with the vertical components of the stresses exerted on a flux rope. In considering the writhing of the flux rope, we also have to consider the horizontal components of the stresses, which are illustrated in Figure 9a.

Initially, the *net* force exerted on the constant-r surface of the flux rope (associated [see Equation (5)] with $\mathcal{T}_{rr}$) is purely vertical, so we examine the stresses on the constant-ζ surface. Initially the $\mathcal{T}_{\zeta\zeta}$ component of the stress tensor produces a *net* force (from the pair of constant-ζ surfaces) with only a vertical component, and it is the $\mathcal{T}_{\zeta\theta}$ component that can produce a net horizontal force. The force associated with the $\mathcal{T}_{\zeta\theta}$ component is in the θ-direction (a tangential stress), as is shown in Figure 9a. After examining the stresses on the constant-ζ surface of the flux rope in Equation (5), we find that the resulting torque about the rotation axis (defined by the vertical green line in Figure 9a) is proportional to the distance from the rotation axis, s, and to the magnitude of the force $\vec{\mathbf{F}}_\theta$, which is proportional to $|B_\theta|$ as evident in Equation (5) (if we assume that B_ζ does not vary over the constant-ζ surface). Thus if the product $|B_\theta s|$ is greater in the upper half of the constant-ζ surface than in the lower half, then the magnitude of the torque exerted by the tangential stress will be greater in the upper half than in the lower half. $|B_\theta|$ is smaller in the upper half than in the lower half of the rope, and Figure 9a shows that s is greater in the upper half. In fact, $|B_\theta|$ is inversely proportional to the radius of curvature, R, of the flux rope at the constant-ζ surface, and it

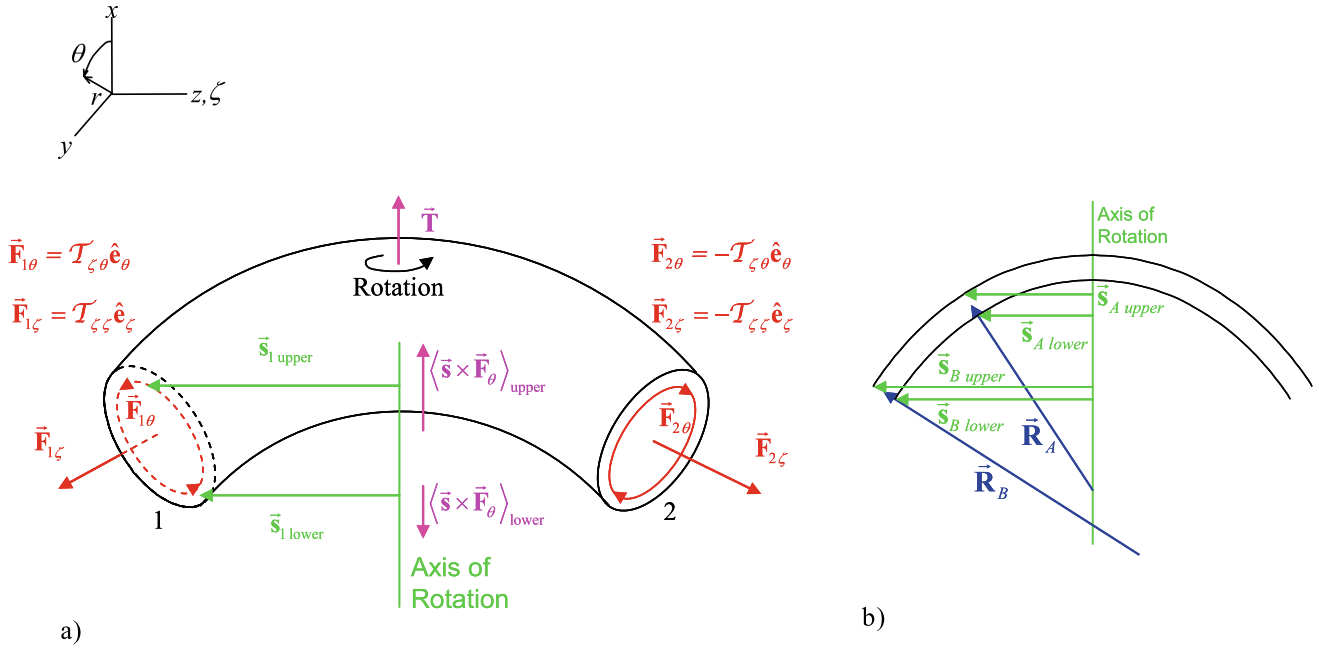

Figure 9 (a) Writhing in the helical stage of the kink instability. The rotation axis, about which torques are shown in this example is parallel to the net torque vector, **T**, and the forces per unit area on the $\zeta =$ constant surfaces are labeled by **F** and specified in terms of the elements of the total stress tensor given in the text. The relative magnitudes of the two torques shown are based on assumptions about the relative magnitudes of $\vec{\mathbf{R}}_{\mathrm{upper}}$ and $\vec{\mathbf{R}}_{\mathrm{lower}}$ and of $\vec{\mathbf{F}}_{\theta\mathrm{upper}}$ and $\vec{\mathbf{F}}_{\theta\mathrm{lower}}$. Note that $\vec{\mathbf{F}}_{1\zeta}$ has a component into the plane of the diagram, while $\vec{\mathbf{F}}_{2\zeta}$ has a component out of the plane. (b) Flux rope with varying radius of curvature, R, with R increasing from the top toward the legs of the flux rope. The distance from the rotation axis is represented by s; the radii, r, measured from the axis of rotation (green vertical line) are shown for two cases of differing radius of curvature.

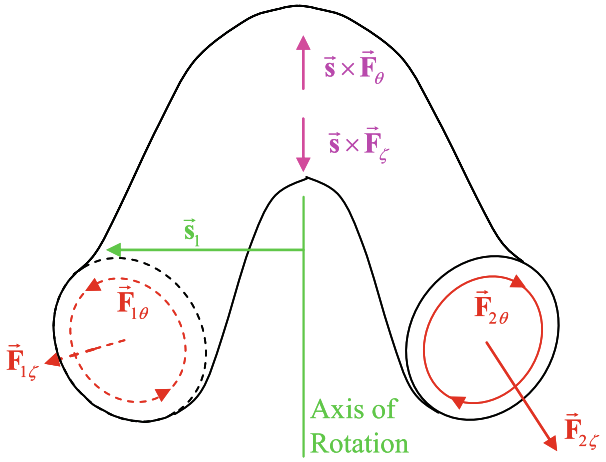

Figure 10 Flux rope of Figure 9a after writhing has begun. The normal forces per unit area ($\vec{\mathbf{F}}_{1\zeta}$ and $\vec{\mathbf{F}}_{2\zeta}$) on the constant-$\zeta$ surfaces now have components perpendicular to the original vertical plane of the flux rope as defined by the flux rope axis in Figures 8 and 9.

can be shown (see Figure 9b, where the radius of curvature is shown for the axis of the flux rope, *i.e.*, at $r = 0$) that if the radius-of-curvature vector, $\vec{\mathbf{R}}$, has its origin on the rotation axis ($\vec{\mathbf{R}}_A$ in Figure 9b), then s is directly proportional to R. In this special case, there is no net torque arising from the $\mathcal{T}_{\zeta\theta}$-component of the stress tensor. If, however, the origin of $\vec{\mathbf{R}}$ is located beyond the axis of rotation ($\vec{\mathbf{R}}_B$ in Figure 9b), then the torque from the upper half of the constant-ζ surface will be greater in magnitude than that from the lower half. Even if there is little or no net torque near the top of a kink-unstable expanding flux rope, as one moves toward the legs of the flux rope, the radius of curvature will increase significantly, and there will be a significant net torque.

Once writhing has started to occur, we consider one last schematic representation of the flux rope, after the effects of the rotation of part of it have begun (Figure 10). Because we assume that the flux rope feet are held fixed, the normal vectors to the constant-ζ surfaces now have a component perpendicular to the original vertical plane defined by the flux rope axis prior to writhing (see Figures 7c and 9a). Recalling from Figure 9a that $\vec{\mathbf{F}}_{1\zeta} = \mathcal{T}_{\zeta\zeta}\hat{\mathbf{e}}_\zeta$ and $\vec{\mathbf{F}}_{2\zeta} = -\mathcal{T}_{\zeta\zeta}\hat{\mathbf{e}}_\zeta$, and assuming that $B_\zeta^2 > B_\theta^2 + 2\mu_0 p$ [*i.e.*, the tension force per unit area dominates the magnetic and plasma pressures; see Equation (5)], it follows that the net effect of $\vec{\mathbf{F}}_\zeta$ on the constant-ζ surfaces is to counteract the writhing owing to the action of $\vec{\mathbf{F}}_\theta$.

References

Alexander, D., Liu, R., Gilbert, H.R.: 2006, *Astrophys. J.* **653**, 719.
Amari, T., Luciani, J.F., Aly, J.J., Tagger, M.: 1996, *Astrophys. J.* **466**, L39.
Amari, T., Luciani, J.F., Aly, J.J., Mikic, Z., Linker, J.: 2003, *Astrophys. J.* **595**, 1231.
Antiochos, S.K., Klimchuk, J.A.: 1991, *Astrophys. J.* **378**, 372.
Antiochos, S.K., DeVore, C.R., Klimchuk, J.A.: 1999, *Astrophys. J.* **510**, 485.
Anzer, U.: 1968, *Solar Phys.* **3**, 298.
Anzer, U.: 1989, *Dynamics and Structures of Quiescent Solar Prominences*, Reidel, Dordrecht, 143.
Aulanier, G., Démoulin, P., Grappin, R.: 2005, *Astron. Astrophys.* **430**, 1067.
Baty, H.: 2001, *Astron. Astrophys.* **367**, 321.
Berger, M.A.: 1999, *Plasma Phys. Control. Fusion* **41**, B167.
Berger, M.A., Field, G.B.: 1984, *J. Fluid Mech.* **147**, 133.
Biskamp, D.: 1993, *Nonlinear Magnetohydrodynamics*, Cambridge University Press, Cambridge.
Boyd, T.M.J., Sanderson, J.J.: 2003, *The Physics of Plasmas*, Cambridge University Press, Cambridge.

Crifo, F., Picat, J.P., Cailloux, M.: 1983, *Solar Phys.* **83**, 143.
Fan, Y.: 2005, *Astrophys. J.* **630**, 543.
Fan, Y., Gibson, S.: 2004, *Astrophys. J.* **609**, 1123.
Fong, B.H., Hurricane, O.A., Cowley, S.C.: 2001, *Solar Phys.* **201**, 93.
Gerrard, C.L., Arber, T.D., Hood, A.W., Van der Linden, R.A.M.: 2001, *Astron. Astrophys.* **373**, 1089.
Gibson, S.E., Fan, Y.: 2006, *Astrophys. J.* **637**, L65.
Gibson, S.E., Low, B.C.: 2000, *J. Geophys. Res.* **105**, 18187.
Gibson, S.E., Fan, Y., Mandrini, C., Fisher, G., Démoulin, P.: 2004, *Astrophys. J.* **617**, 600.
Gibson, S.E., Foster, D., Burkepile, J., de Toma, G., Stanger, A.: 2006, *Astrophys. J.* **641**, 590.
Gilbert, H.R., Holzer, T.E., Burkepile, J.T., Hundhausen, A.J.: 2000, *Astrophys. J.* **537**, 503.
Gilbert, H.R., Holzer, T.E., Low, B.C., Burkepile, J.T.: 2001, *Astrophys. J.* **549**, 1221.
Goedbloed, H., Poedts, S.: 2004, *Principles of Magnetohydrodynamics*, Cambridge University Press, New York.
Hood, A.W.: 1992, *Plasma Phys. Control. Fusion* **34**, 411.
Hood, A.W., Priest, E.R.: 1979, *Solar Phys.* **64**, 303.
Howard, R.A., Sheeley, N.R., Koomen, M.J., Michels, D.J.: 1985, *J. Geophys. Res.* **90**, 8173.
Hundhausen, A.J.: 1988, In: Pizzo, V., Sime, D.G., and Holzer, T.E. (eds.) *Proc. Sixth International Solar Wind Conference, NCAR TN-306* **1**, 181.
Isenberg, P.A., Forbes, T.G., Démoulin, P.: 1993, *Astrophys. J.* **417**, 368.
Ji, H., Wang, H., Schmahl, E.J., Moon, Y.-J., Jiang, Y.: 2003, *Astrophys. J.* **595**, L135.
Kippenhahn, R., Schlüter, A.: 1957, *Z. Astrophys.* **43**, 36.
Kliem, B., Török, T.: 2006, *Phys. Rev. Lett.* **96**, 255002.
Kuperus, M., Raadu, M.A.: 1974, *Astron. Astrophys.* **31**, 189.
Lin, J., Forbes, T.G.: 2000, *J. Geophys. Res.* **105**, 2375.
Lin, J., Soon, W., Baliunas, S.L.: 2003, *New Astron. Rev.* **47**, 53.
Lin, J., Forbes, T.G., Isenberg, P.A., Démoulin, P.: 1998, *Astrophys. J.* **504**, 1006.
Linker, J.A., Mikić, Z., Riley, P., Lionello, R., Odstrcil, D.: 2003. In: *Proceedings of the Tenth International Solar Wind Conference* **679**, 703.
Linton, M.G., Longcope, D.W., Fisher, G.H.: 1996, *Astrophys. J.* **469**, 954.
Liu, R., Alexander, D., Gilbert, H.: 2007, *Astrophys. J.* **661**, 1260.
Low, B.C.: 1996, *Solar Phys.* **167**, 217.
Low, B.C., Hundhausen, J.R.: 1995, *Astrophys. J.* **443**, 818.
Martin, S.F.: 1989, In: Ruždjak, V., Tandberg-Hanssen, E. (eds.) *Dynamics of Quiescent Prominences*, Springer, Berlin, 1.
Mouradian, Z., Soru-Escaut, I.: 1989, *Astron. Astrophys.* **210**, 410.
Munro, R.H., Gosling, J.T., Hildner, E., MacQueen, R.M., Poland, A.I., Ross, C.L.: 1979, *Solar Phys.* **61**, 201.
Parker, E.N.: 1975, *Astrophys. J.* **201**, 494.
Plunkett, S.P., Vourlidas, A., Šimberová, S., Karlický, M., Kotrč, P., Heinzel, P., *et al.*: 2000, *Solar Phys.* **194**, 371.
Pneuman, G.W.: 1983, *Solar Phys.* **88**, 219.
Priest, E.R.: 1983, *Solar Phys.* **86**, 33.
Priest, E.R., Forbes, T.G.: 2000, *Magnetic Reconnection*, Cambridge University Press, Cambridge.
Raadu, M.A.: 1972, *Solar Phys.* **22**, 425.
Romano, P., Contarino, L., Zuccarello, F.: 2003, *Solar Phys.* **214**, 313.
Rust, D.M., Kumar, A.: 1994, *Solar Phys.* **155**, 69.
Rust, D.M., LaBonte, B.J.: 2005, *Astrophys. J.* **622**, L69.
Sakurai, T.: 1976, *Astron. Soc. Japan* **28**, 177.
Schmieder, B., Aulanier, G., Mein, P., López-Ariste, A.: 2006, *Solar Phys.* **238**, 245.
Sheeley, N.R. Jr., Bohlin, J.D., Brueckner, G.E., Purcell, J.D., Scherrer, V.E., Tousey, R., *et al.*: 1975, *Solar Phys.* **45**, 377.
St. Cyr, O.C., Webb, D.F.: 1991, *Solar Phys.* **136**, 379.
St. Cyr, O.C., Burkepile, J.T., Hundhausen, A.J., Lecinski, A.R.: 1999, *J. Geophys. Res.* **104**, 12493.
Sturrock, P.A., Weber, M., Wheatland, M.S., Wolfson, R.: 2001, *Astrophys. J.* **548**, 492.
Tandberg-Hanssen, E.: 1974, *Solar Prominences*, Reidel, Dordrecht, 12.
Tandberg-Hanssen, E.: 1995, *Solar Prominences*, Kluwer Academic, Dordrecht, 199.
Tang, F.: 1987, *Solar Phys.* **107**, 233.
Taylor, J.B.: 1974, *Phys. Rev. Lett.* **33**, 1139.
Taylor, J.B.: 1986, *Rev. Mod. Phys.* **58**, 741.
Török, T., Kliem, B.: 2003, *Astron. Astrophys.* **406**, 1043.
Török, T., Kliem, B.: 2005, *Astrophys. J.* **630**, L97.

Török, T., Kliem, B.: 2007, *Astron. Nachr.* **328**, 743.
Török, T., Kliem, B., Titov, V.S.: 2004, *Astron. Astrophys.* **413**, L27.
Webb, D.F., Hundhausen, A.J.: 1987, *Solar Phys.* **108**, 383.
Williams, D.R., Török, T., Démoulin, P., van Driel-Gesztelyi, L., Kliem, B.: 2005, *Astrophys. J.* **628**, L163.
Zhang, M., Flyer, N., Low, B.C.: 2006, *Astrophys. J.* **644**, 575.
Zhou, G.P., Wang, J.X., Zhang, J., Chen, P.F., Ji, H.S., Dere, K.: 2006, *Astrophys. J.* **651**, 1238.
Zirin, H.: 1988, *Solar Astrophysics*, Cambridge University Press, Cambridge.